Towards a Soft Fingertip with Integrated Sensing and Actuation

Benjamin W. McInroe*, Carolyn L. Chen*, Ken Y. Goldberg, Ruzena Bajcsy, Ronald S. Fearing

***Abstract*— Soft material robots are attractive for safe interaction with humans and unstructured environments due to their compliance and low intrinsic stiffness and mass. These properties enable new capabilities such as the ability to conform to environmental geometry for tactile sensing and to undergo large shape changes for actuation. Due to the complex coupling between sensing and actuation in high-dimensional nonlinear soft systems, prior work in soft robotics has primarily focused on either sensing or actuation. This paper presents SOFTcell, a novel controllable stiffness tactile device that incorporates both optical sensing and pneumatic actuation. We report details on the device's design and implementation and analyze results from characterization experiments on sensitivity and performance, which show that SOFTcell can controllably increase its effective modulus from 4.4kPa to 46.1kPa. Additionally, we demonstrate the utility of SOFTcell for grasping in a reactive control task in which tactile data is used to detect fingertip shear as a grasped object slips, and cell pressurization is used to prevent the slip without the need to adjust fingertip position.**

I. Introduction

There is a growing interest in using soft materials, such as elastomers and polymers, in robots. Two widely recognized advantages of such systems are the ability to deform and change shape in response to internal and external loads, and their low intrinsic stiffness and mass, which makes them especially useful for safe human-robot interaction and operation in delicate environments. Previous studies have explored the capabilities of soft systems in both actuation and sensing [1, 2], and recent progress in soft robots has shown them to be capable of performing challenging tasks, including legged locomotion [3] and dexterous grasping [4].

Design of actuation, sensing, and control of these soft systems remains an active area of research. Common methods of actuation include pneumatic [5] and hydraulic [6] actuation, cable-driven tendon systems [7], smart materials such as shape-memory alloys (SMAs) [8] and dielectric elastomers (DEAs) [9], and chemical reactions [10]. The high dimensional configuration spaces and intrinsic nonlinear dynamics of soft materials present both a challenge for control and an opportunity for extracting rich tactile information from the external environment. Many tactile sensing technologies have been integrated into soft robotic platforms, including fiber optic sensors [11] and flexible electronic sensors [12].

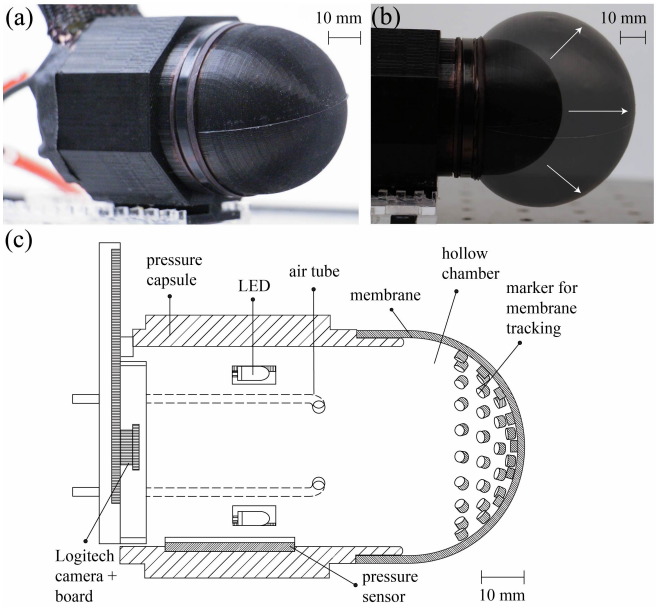

Fig. 1: (a) The Soft Optical Feedback Tactile cell (SOFTcell), a device towards a soft fingertip with integrated sensing and actuation. (b) Pneumatic actuation enables controllable increase of effective modulus and a >200% increase in volume. (c) A cutaway scale diagram of SOFTcell displaying its assembled internal components.

However, the embedding of rigid materials such as conductive wires or tendons in soft components imposes constraints on maximum material strain [13]. This limits the deformation ability of the system, and thus removes a fundamental benefit of soft material robots. To circumvent this limitation of traditional tactile sensors, non-contact sensors for soft systems have been explored [14] in order to decouple the sensing devices from the soft material. For pneumatically-driven systems, one solution that has been explored is using pressure sensing to detect collisions [15]. Image-based tactile sensors, which measure 2-D and 3-D deformation fields from image data, present another attractive alternative. Spatially rich tactile information enables contact localization and registration of finer contact dynamics.

Non-contact image-based methods have been previously used to develop soft fingertips for tactile sensing and dexterous manipulation [16]. Begej et. al. [17] designed planar tactile sensors that used cameras to image contact on an elastic membrane. Yamaguchi et. al. [18] developed a low-cost tactile sensor called FingerVision that uses a transparent skin with

This material is based on work supported by Award 31701 from the Office of Naval Research Multidisciplinary University Research Initiative, donations from Siemens, Google, and Amazon Robotics, and the Department of Defense (DoD) through the National Defense Science and Engineering Graduate Fellowship (NDSEG) Program.

B.W. McInroe is with the Biophysics Graduate Group, University of California, Berkeley, CA 94720 USA bmcinroe@berkeley.edu

C.L. Chen, R. Bacjsy, and R.S. Fearing are with the Department of Electrical Engineering and Computer Science, University of California, Berkeley, CA 94720 USA {carolyn.chen, bajcsy, ronf}@eecs.berkeley.edu

K.Y. Goldberg is with the Department of Industrial Engineering and Operations Research, University of California, Berkeley, CA 94720 USA goldberg@berkeley.edu

*These authors contributed equally to this work.

tracking markers to collect static and dynamic information. Hristu et. al. [19] built a gel-filled fingertip with markers and a fixed camera that measured displacements of markers on the fingertip surface to reconstruct 3-D geometries. A related device is the GelSight sensor, a high resolution tactile sensor with an elastomer gel membrane coated with reflective material, which uses a coaxial camera and illumination by multiple LEDs to capture height maps of the surface deformation [20]. Chorley et. al. [21] developed a similar device to that of [19] called the TacTIP sensor, which includes pins on the surface of the gel-filled membrane inspired by dermal papillae in human fingertips. The WORMtip sensor [22] replaced the gel-filled membrane with a pneumostatic vessel consisting of a dielectric elastomer (DEA) sheet on one end and an elastic membrane on the other. Actuation of the DEA allowed the surface to extend and retract for palpation tasks. However, kilovolt ranges are needed for DEAs in comparison to pnuematically actuated robots that can operate through miniaturized compressors and valves that typically run at household voltages [3].

Recent work has explored the possibility of function-selectable tactile sensing through programmable morphology [23]. However, the potential for both multimodal sensing and actuation in soft tactile sensing devices remains underexplored. Stilli et. al. [15] begins to bridge this gap by proposing to use pressure sensing of pneumatically-driven robotic arms to detect collisions. We aim to continue to reveal the capabilities of soft actuated tactile devices through the development and study of a new pneumatically-actuated soft tactile sensing device, the SOFTcell (Soft Optical Feedback Tactile cell). Through the combination of valve-controlled pneumatic actuation and image-based sensing, we controllably exploit the intrinsic conformability of a soft membrane at low internal pressure for large deformation tactile sensing and the increased effective modulus at high internal pressure for large load actuation. We show that the functionality of the system is multimodal, with different pressurization states allowing for different functionality such as improved tactile sensitivity or increased contact forces.

We further explore the utility of SOFTcell's multimodal sensing and actuation in practical applications by demonstrating shear detection and grasp adjustment in a constrained manipulation task. SOFTcell holds an object against a static wall, and the mass of the object is slowly increased. When shear is detected due to the object slipping against the wall, the cell pressure is increased, stabilizing the object without the need to adjust fingertip position.

The paper is organized as follows. Section II discusses the design and fabrication of SOFTcell, including a discussion of the general work flow and image processing algorithms used for tactile feedback. Section III presents a theoretical analysis of SOFTcell in the linear elastic regime and describes the fundamental physical principles governing the controllable sensing and mechanical stiffness capabilities of the device. Section IV presents the results of systematic experimental characterization of SOFTcell and discusses empirical measurements of variable stiffness and tactile sensitivity. Section V presents empirical measurements for model validation and describes preliminary application-domain demonstrations in reactive grasping that employ both high resolution sensing and large deformation actuation. Section VI further discusses the utility of SOFTcell and coupled soft sensor/actuator systems, followed by a discussion of future directions.

Summary of Contributions

This paper makes the following contributions:

1) The design and fabrication of SOFTcell, a controllable stiffness device that is capable of both spatiotemporal tactile sensing and actuation.
2) Modeling and characterization of SOFTcell's controlled stiffness range and multimodal sensing and actuation features.
3) A demonstration of the application of SOFTcell in a reactive control task, which requires both spatiotemporal tactile data and actuation to exert controlled forces on the environment.

II. System Design and Fabrication

A. Design and Fabrication

1) Tip: The underside of the silicone skin closely resembles that of [21], a pattern of cylinders that are inspired by Meissner's corpuscle mechanoreceptors for sensitive tactile responses. This patterning was chosen primarily due to its area-preserving characteristics, an important feature to simplify image processing for a membrane that is capable of nontrivial changes in surface area. As shown in several relevant works on tactile optical sensors ([18, 22, 24–26]), tracking features of deformable skin such as these synthetic markers allows for acquisition of tactile data, e.g. dynamic information like shearing or geometric information like convexity of an object. We designed and printed a hemispherical multiple-part mold to cast the tip out of platinum-catalyzed EcoFlex 50 Silicone. In order to ensure uniform thickness throughout the membrane, a vacuum chamber was used to remove gas from the uncured silicone. The cured silicone skin has a thickness of 1.7 mm and an inner radius of 21.23 mm. Each cylinder is 2mm long with a radius of 1mm, and the cylinders are distributed uniformly across the underside of the hemisphere with a center-to-center distance of at least 7mm. To make the cylinder features visually striking, black silicone pigment was mixed into the EcoFlex and the cylinder tips were painted with white silicone-based paint. The silicone membrane was fastened onto the rim of the camera and pressure capsule with cable ties.

2) Camera and Pressure Capsule: A Logitech HD C310 Webcam, centered and facing towards the underside of the silicone skin, was secured at the bottom of a capsule 3D-printed out of Polylactic Acid (PLA). The camera was positioned 67 mm away from the rim of the capsule to optimize for its focal length and field of view. A pressure/temperature MS5803-14BA sensor with an accuracy of ± 0.02 kPa under pressures up to 1400 kPa in room temperature was also fastened inside the capsule. Flexible pipes embedded into the capsule's walls act as channels between solenoid valves connected to an air

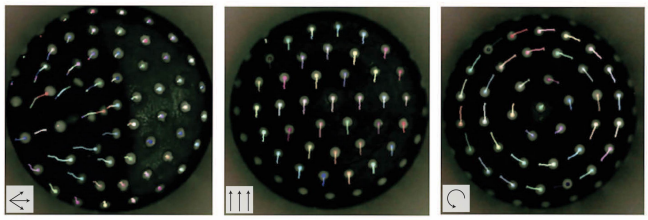

Fig. 2: Examples of raw images captured by the internal camera, overlaid with the traces of the trajectories of the markers. Different colors are assigned to distinguish different marker traces. Arrows found in the bottom-left corners serve to illustrate the general directional motion of the markers. (a) The membrane is indented radially on the left side by a spherical probe (see Figure 4). (b) The membrane shears in contact with a flat surface moving upwards. (c) The membrane experiences torsion while in contact with a twisting flat surface.

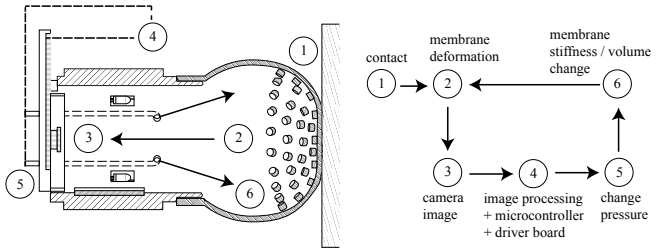

Fig. 3: General system workflow. Contacts are transmitted as images via the internal camera and further modified by the image processing scheme. The vectors of marker displacements are then interpreted as tactile feedback, e.g., a detected membrane shear. A central computer computes a command, e.g., increase pressure, in response to the vectors, which is relayed to the microcontroller. The microcontroller sends a PWM signal to the solenoid valves, which in turn change the air pressure supplied to the SOFTcell. This subsequently changes the volume and stiffness of the elastic tip. The change in volume is captured by the internal camera as well, demonstrating proprioceptive capabilities of the SOFTcell.

compressor and the capsule's interior, allowing the capsule to be pressurized. The capsule was sealed with hot glue to minimize leakage of air.

3) Composite Setup: The device consists of the hemispherical silicone membrane attached to the pressure capsule, with LED's for lighting and a camera at the bottom of the cell for sensing. A cutaway diagram of the composite setup of SOFTcell and its internal components is illustrated in Figure 1. The entire cost of the SOFTcell, including all sensors and materials, amounted to under 100 USD.

B. System Configuration

The SOFTcell is connected to a compressor pressurized to 410 kPa, and the solenoid valves that modulate air flow from the compressor into the SOFTcell are controlled by Matrix driver boards. The valves are fitted with orifices that leak air so that pressure can be increased and decreased by a single Pulse Width Modulated (PWM) solenoidal valve [27].

An Arduino Micro microcontroller relays PWM commands to the valve driver boards. The Micro and camera are both connected to a central computer. Application demonstrations reported in Section V-B, which require basic feedback from the camera images, involve serial communication between a Python script and the Micro.

For the characterization experiments reported in Section IV, an ATI 45 six-axis force-torque transducer is oriented in front of the SOFTcell in various configurations in order to measure the force and torque output of the device. A second Arduino microcontroller is used to receive data from the MS5803-14BA pressure/temperature sensor and an ATI F/T Data Acquisition (DAQ) device is used to relay the measurements from the force-torque transducer to a MATLAB script, which we use to further analyze the data.

C. Tactile Image Processing

We rely on the internal camera data alone for tactile feedback. At first, we considered using pressure data from the MS5803-14BA sensor in parallel with the image data, as pressure has been used in some prior work to determine collisions of an inflatable robot arm [15]. However, through our own investigation, we determined that pressure signals show no substantial change that could robustly distinguish fine membrane perturbations such as those depicted in Figure 2, and thus are insufficient to be used for tactile data. We incorporate the pressure sensor in the device solely for device characterization.

We explored using common image processing techniques to extract relevant tactile information from the camera images. Our general preprocessing scheme began by low-pass filtering the image with a Gaussian blur, grey-scaling the image, and applying an Otsu adaptive threshold to binarize the image. Erosion and dilation was applied to remove false positive identifications of the cylindrical markers due to specular highlights, and further cleaning was performed using connected component analysis. OpenCV's `SimpleBlobDetector` was used to find the centroids of the white markers. The centroids were then tracked with OpenCV's implementation of optical flow for a sparse feature set using the Lucas-Kanade method with pyramids (`calcOpticalFlowPyrLK`).

From the optical flow output, we can calculate a set of vectors describing the translations of the markers from a previous frame. These vectors can then be used for dynamic tracking of the elastic membrane, inferring contact conditions, and detecting membrane shear. In Section V-B, we demonstrate these sensing modalities at 30Hz in experiment. Figure 2 shows example trace vectors as the membrane is perturbed from the outside, and Figure 3 illustrates the workflow of the composite system.

III. Model of SOFTcell

We preface our experiments with a brief discussion of theoretical motivation. Intuitively, one expects that the SOFTcell membrane should become more rigid as internal pressure increases. The mechanical properties of SOFTcell are a function of both the thermodynamic state of the internal air and the strain state of the elastic membrane. Furthermore, contact forces and displacements of the membrane will depend

on the contact geometry.

For small deformations about an equilibrium state, we assume that the mechanical response of SOFTcell can be modeled as that of an equivalent linearly elastic solid sphere subject to the same contact conditions. This equivalent sphere has an associated elastic modulus that we refer to as the effective modulus of SOFTcell, E^*. This effective modulus provides a useful predictive measure of SOFTcell's variable stiffness. The mechanics of hyperelastic materials under large deformations are complex and nonlinear. Previous work by Vella et. al. studied models of the indentation of pressurized spherical shells, demonstrating the nonlinear relationship between effective modulus and internal pressure [28]. In IV, we show experimentally that the effective modulus provides a good approximation to the mechanical response of SOFTcell.

In our characterization experiments, we consider indentation of SOFTcell's membrane by simple geometries. From Hertz contact theory for the frictionless contact between elastic spheres, the load force F and indentation depth δ are related by [29]:

$$F = \frac{4}{3}\left(\frac{1-\nu_1}{E_1}+\frac{1-\nu_2}{E_2}\right)^{-1}\left(\frac{1}{R_1}+\frac{1}{R_2}\right)^{-1/2}\delta^{3/2} \quad \text{(III.1)}$$

where ν_i, E_i, and R_i are the Poisson's ratio, elastic modulus and radius for sphere $i \in \{1,2\}$. We will restrict our experiments to the case $E_1 << E_2$, that is, the deformation of the object in contact with SOFTcell is negligible. We can then define the effective modulus of SOFTcell under a specified pressure state and contact condition as,

$$E^* = \frac{3F}{4\delta^{3/2}}\left(\frac{1}{R_1}+\frac{1}{R_2}\right)^{\frac{1}{2}}(1-\nu) \quad \text{(III.2)}$$

Here, ν is the Poisson's ratio of the equivalent elastic sphere ($\nu = 0.5$ for ideal rubber). This result holds for plane contact in the limit as $R_2 \to \infty$.

IV. Experimental Characterization of System

We characterize the variable stiffness and sensing capabilities of SOFTcell through a series of controlled experiments. In Section IV.A, we demonstrate the dependency of sensor mechanical stiffness, quantified here as effective modulus (Eqn. III.2) on internal pressure. In Section IV.B, we explore the force applied to a fixed object in contact with SOFTcell as internal pressure is periodically increased and decreased. Section IV.C summarizes our sensitivity analysis of SOFTcell's force sensing capabilities. All recorded values for pressures are gauge pressure.

A. Variable Stiffness

We use an ATI 45 six-axis force-torque transducer with a mounted 1.9 cm radius spherical probe to measure contact forces and torques on the SOFTcell. In these experiments, the SOFTcell is inflated to a fixed initial pressure and then quasistatically indented by the probe at a series of fixed indentation depths, both coaxially with the device and off axis by a 45 deg angle (Fig. 4) . Pressure and temperature within the cell are recorded, and the reaction forces and torques on the ATI sensor are recorded at mechanical and thermal equilibrium of SOFTcell. The results of these experiments are shown in Figure 5. We find that while the load forces on SOFTcell show similar monotonic increases with indentation depth, higher pressures result in larger load forces for the same indentation. The coaxial contact experiments are repeated with a planar probe.

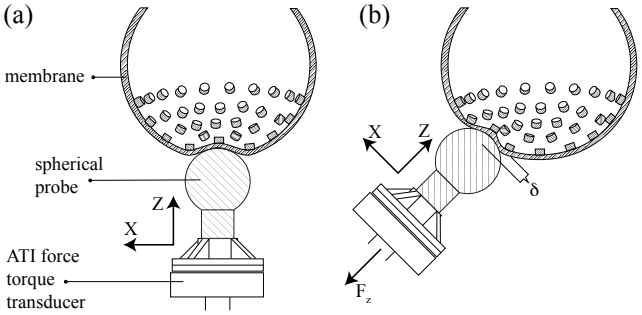

Fig. 4: A schematic representation of the mechanical stiffness characterization experiments. (a) Coaxial contact with the spherical probe. (b) Radial contact at an angle of $\frac{\pi}{4}$.

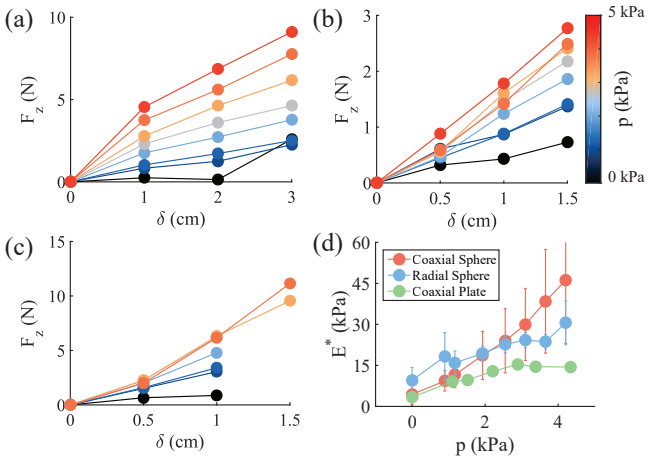

Fig. 5: The results of the mechanical stiffness characterization experiments described in IV.A. (a) Coaxial contact with a spherical probe. (b) Radial contact ($\frac{\pi}{4}$) with a spherical probe. (c) Coaxial contact with a planar probe. At low pressures and higher indentations δ, the planar probe contacted the rim of the pressure capsule, so forces were not recorded. (d) SOFTcell's effective modulus increases as the internal pressure is increased.

Following Eqn. III.2, we compute the effective moduli for SOFTcell at different internal pressure states. The results are shown in Figure 5. As hypothesized, E^* increases with pressure for all contact scenarios.

B. Dynamic Loading and Hysteresis

Using the same experimental apparatus as in the previous section, we measure the time-varying force imparted on a fixed probe as SOFTcell undergoes cyclic pressurization. The probe is placed so that it is initially in point contact with the membrane of SOFTcell so that there is no deformation of the membrane when the internal pressure of SOFTcell is the

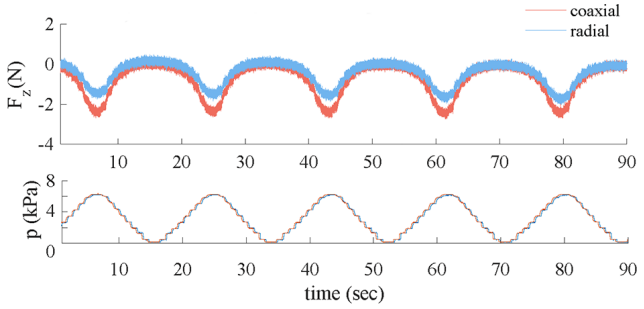

Fig. 6: Comparison of coaxial and radial contact forces exerted by SOFTcell onto a fixed force-torque sensor. The internal gauge pressure is varied between 0 and 6.14 kPa in a triangle wave-like oscillation.

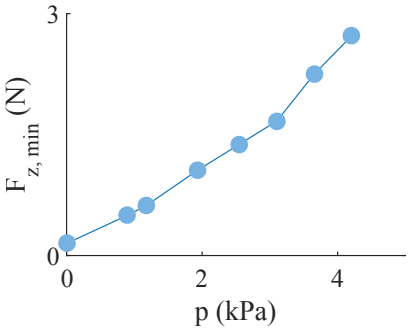

Fig. 7: The minimum detectable force ($F_{z,min}$) for coaxial contact with the spherical probe vs. the internal pressure of SOFTcell.

same as the ambient atmospheric pressure. The duty cycle of the solenoidal valve connected to SOFTcell is then increased and decreased from 0% to 100% as a triangle wave with a period of 17.5 sec (Fig. 6). The force measured on the load cell closely tracks the triangle wave signal, showing the responsiveness of SOFTcell's actuation. Furthermore, we find that after 222 cycles at 1 Hz, the load force remains consistent with a maximum peak of $1.17 \pm 1.66E-4$ N, showing negligible hysteresis and demonstrating the repeatability of SOFTcell's actuation capabilities.

C. Sensitivity

We characterize the effect of controlling the internal pressure of SOFTcell on its sensing capabilities. For the previously decribed spherical probe, the minimum detectable coaxial deflection of SOFTcell above the camera's static noise is found to be 0.6 mm. For a small deflection, we linearize our empirical measurement of $F_z(\delta)$ (Fig. 5) at the origin to estimate minimum force resolution. We find that minimum detectable force increases with internal pressure so that smaller contact forces are detectable at lower pressures (Fig. 7).

V. Towards Reactive Grasping

We now utilize a different experimental setup as illustrated in Figure 8 in order to achieve two goals. We first aim to validate the Hertz contact and effective modulus model of SOFTcell through a simple shear experiment in Section V-A,

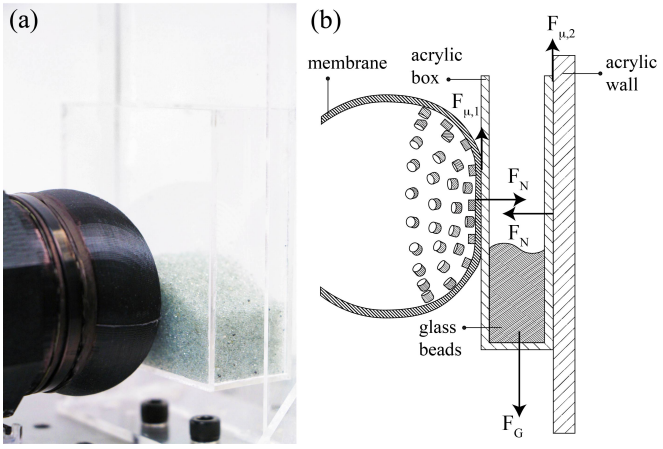

Fig. 8: The experimental setup for Section V-A and Section V-B. (a) SOFTcell pushes a box of glass beads against a wall, applying sufficient normal force to counter the effect of gravity; (b) a free-body diagram of forces involved in this experimental setup.

and we follow this with an implementation towards simple reactive grasping in Section V-B.

A. Model Validation

For this experimental setup, we fix SOFTcell such that its tip, under atmospheric pressure, is 20.25 mm from a vertical acrylic wall (see Figure 8). An empty 28.37 mm wide by 76.2 mm $\times$ 76.2 mm acrylic box with mass of 31.6 g is suspended between the uninflated SOFTcell and the wall, causing SOFTcell's initial normal membrane deflection (δ) to be 8.12 mm. SOFTcell maintains planar contact with the box throughout the experiment. The forces from the elastic membrane are sufficient at internal atmospheric pressure to counter the weight of the empty box.

We vary the internal pressure state of SOFTcell ($0-3$ kPa). For each pressure state, we continuously increase the mass of the empty box by adding 0.8 mm diameter / 670.2 μg glass beads. As the load increases, the gravitational force overcomes the static frictional force between the box and the wall, causing it to slip and the SOFTcell membrane to shear. We distinguish membrane shear from other perturbations such as pure indentation through the displacement vectors of the internal markers. Our heuristic determines shear if the standard deviation of the angular displacement is below an experimentally-determined conservative threshold (i.e., the displacement vectors are all within some margin in the same direction). Once a shear in the membrane is detected, we measure the mass of the box and repeat this process for a total of ten trials per pressure state (Fig. 11).

To visualize membrane shear displacement, we use SciPy's radial basis function interpolation class to approximate a denser map of displacements from the sparse set of displacements extracted from the image. A contour plot of isodisplacement level curves can then be calculated from this dense map of interpolated displacements, providing an approximation of the global membrane motion and deformation. Figure 9 depicts representative isodisplacement

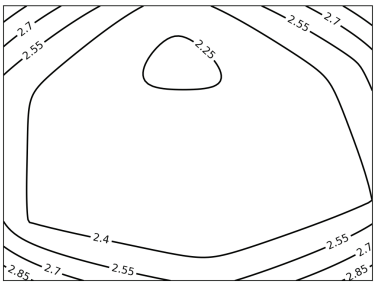

p = 0.34 kPa

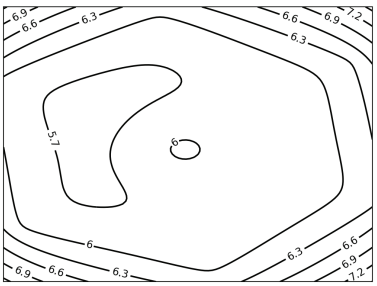

p = 2.21 kPa

Fig. 9: Contours of uniform membrane displacement from SOFTcell sensor data for a 0.8N shear load at different cell pressure states. Displacements are in mm, in the direction of shear. Displacements in the direction normal to shear were negligible for all trials.

contour plots of the membrane shear data measured by SOFTcell during the experiments. Each plot depicts sensor data of membrane deflection in the direction of shear under a shear load of 0.8N. The displacement fields of the membrane in the direction normal to shear were found to be negligible. This is consistent with our assumption motivating the heuristic for shear detection that the direction of shear should be relatively uniform between the markers for a planar coaxial contact.

In addition to visualizing membrane shear from the displacement data, we also plotted the spatial average shear deflections over the membrane against shear load at varying internal pressures in Figure 10. As the shear load increases, SOFTcell detects larger shear deflections. This illustrates, from the clustered data of Figure 10 at different pressure states, given a measured average shear deflection, approximate shear force or load can be inferred.

Finally, from our measurements of box mass at the instance of slip, we estimate the normal force between SOFTcell and the box (F_N). We measure the normal deflection (δ) of the membrane at the center of contact and plot these results in Figure 11. From the Hertz contact model (Eq. III.1), we obtain a prediction for the normal force-deflection relation:

$$F_N(p,\delta) = \frac{4}{6} R(p)^{\frac{1}{2}} E^*(p) \delta^{3/2} \tag{V.1}$$

where $R(p)$ is the tip radius at pressure p, and $E^*(p)$ is the effective modulus, determined empirically through characterization experiments (Fig. 5). We find close agreement

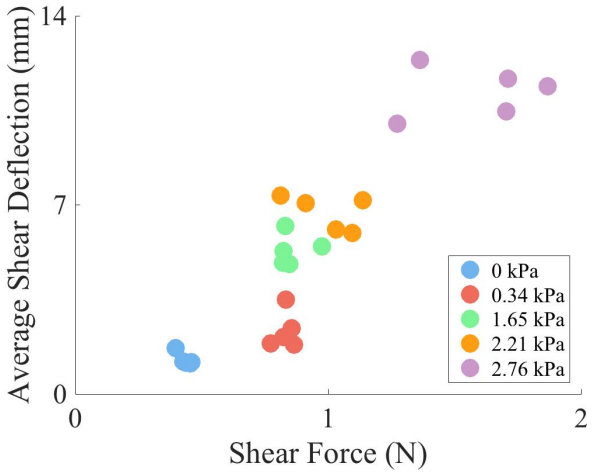

Fig. 10: Average membrane shear deflection measured by SOFTcell for different shear loads at different cell pressure states. Different deflections are measured at different shear loads (depending on the internal pressure state), suggesting that approximate shear load can be inferred from the spatial tactile data.

between our Hertz contact and effective modulus model and empirical results. Deviations between the model and experiment are likely due to nonlinear effects outside of the regime of Hertz contact theory.

B. Task Demonstration

We present preliminary investigation of the potential for SOFTcell to aid in fine manipulation tasks, in particular, with reactive grasping. Specifically, we utilize SOFTcell's spatiotemporal sensing modality to extract contact conditions during a grasp. Membrane shear is measured by the sensor, and the actuation modality is then used to perform a reactive single-finger "grasping" adjustment of an object under varying load.

Measuring shear and slip of objects has been well-studied throughout tactile sensing literature ([25, 30–36]) and a few groups have incorporated this detection into closed-loop control for grasping ([31, 33–36]). Here, we take inspiration from the experiments in [30] and [25] to simulate a grasp between a finger equipped with sensing (SOFTcell) and a stationary wall or "finger" that provides structural support, using the identical experimental setup in Section V-A (Figure 8). SOFTcell's actuation capability allows it to additionally adjust the strength of the grasp based on inferred grasp quality from sensory data.

For this demonstration, we begin with the same initial conditions as in Section V-A, with an internal pressure state matching atmospheric pressure. SOFTcell is at an identical distance from the acrylic wall as before, and the same acrylic box is suspended between SOFTcell and the wall. We vary the load by pouring glass beads into the box, similar to an experiment presented in [36]. It is expected that at some critical mass (dependent on the internal pressure of SOFTcell), the membrane will shear as the box transitions from static to kinetic friction contact with the acrylic wall. When a shear

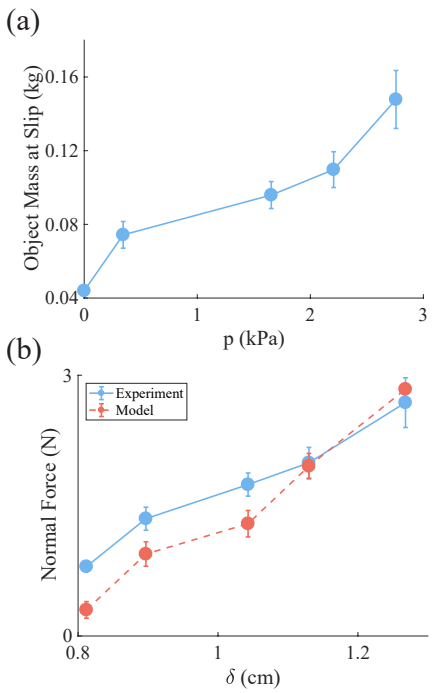

Fig. 11: Results of the membrane shear experiments (Section IV.E). (a) The mass of the grasped object at the point of slip / detected shear vs. the pressure state of SOFTcell. (b) Measured normal force vs. normal deflection compared to theoretical predictions from the effective modulus Hertz contact model with measured parameters. Error bars show 95% confidence interval.

is detected, the pressure within SOFTcell is increased to re-grasp the object and prevent slip.

As we vary the load of the box, SOFTcell successfully fine-tunes the grasp in real-time by incrementally increasing its internal pressure and subsequently the applied normal force to the box upon each detection of a shear, countering the new gravitational loads. We set the maximum internal pressure at $4kPa$ so that SOFTcell's membrane would not contact anything other than the box (as it grows larger, it has the potential to touch the platform on which it is mounted). At the maximum internal pressure of $4kPa$, SOFTcell is able to "grasp" a full box of glass beads with a mass of 210.2 g. A demonstration of this reactive grasping task is captured in the corresponding video to this paper.

VI. Discussion and Future Work

In this paper, we presented the design and fabrication of SOFTcell, a low-cost variable stiffness pneumatic device capable of multimodal tactile sensing and actuation. We demonstrated that through a single control input (the pressure state within SOFTcell), we can control both the range of contact forces that can be detected through tactile sensing and the effective modulus for actuation. We also demonstrated how control of internal pressure allows for SOFTcell to operate multifunctionally through different sensing and actuation primitives, such as through increased sensitivity at lower pressure states and increased grasping force at higher pressure states. We developed a simple effective modulus model of the device based on Hertz contact theory and validated the model empirically. This effective modulus model enables estimation of the relationship between contact force and membrane strain depending on the cell pressure and contact conditions. Finally, we investigate the utility of SOFTcell in a reactive grasping task, demonstrating shear detection and variable stiffness to improve contact.

There are numerous possible directions for future work. One direct application of the SOFTcell would be in active tactile object and environmental exploration. Figures 2 and 9 provide examples of the rich image data that can be acquired from observing interactions of the elastic membrane with the environment. Since the SOFTcell was designed to be scalable, it could be miniaturized into a fingertip, although its size would ultimately be constrained by the parameters of the internal camera. With this data, we would like to explore basic tactile sensing tasks such as detecting incipient slip [30], categorizing material textures, tracing seams and object boundaries [37], reconstructing object geometries, and estimating material stiffness through impedance matching. It would be important to also characterize the resolution of details captured by the images when varying the stiffness of the membrane, as this would evaluate how SOFTcell augments its multimodal tactile capabilities through variable stiffness.

Finally, we are also interested in using SOFTcell as an end effector for legged locomotion. Substrate properties vary dramatically in natural environments, necessitating multifunctional appendages for legged locomotion. Using SOFTcell as a robotic appendage could improve robot mobility by controlling stiffness to actively explore surface materials [38] and to help gain traction in challenging terrain.

Acknowledgment

The authors would like to thank our colleagues who provided helpful feedback and suggestions, in particular Robert Matthew and Matthew Matl.

References

[1] D. Rus and M. T. Tolley, "Design, fabrication and control of soft robots", *Nature*, vol. 521, no. 7553, p. 467, 2015.

[2] L. Wang and F. Iida, "Deformation in soft-matter robotics: A categorization and quantitative characterization", *IEEE Robotics & Automation Magazine*, vol. 22, no. 3, pp. 125–139, 2015.

[3] M. T. Tolley, R. F. Shepherd, B. Mosadegh, K. C. Galloway, M. Wehner, M. Karpelson, R. J. Wood, and G. M. Whitesides, "A resilient, untethered soft robot", *Soft Robotics*, vol. 1, no. 3, pp. 213–223, 2014.

[4] F. Ilievski, A. D. Mazzeo, R. F. Shepherd, X. Chen, and G. M. Whitesides, "Soft robotics for chemists", *Angewandte Chemie*, vol. 123, no. 8, pp. 1930–1935, 2011.

[5] B. Mosadegh, P. Polygerinos, C. Keplinger, S. Wennstedt, R. F. Shepherd, U. Gupta, J. Shim, K. Bertoldi, C. J. Walsh, and G. M. Whitesides, "Pneumatic networks for soft robotics that actuate rapidly", *Advanced Functional Materials*, vol. 24, no. 15, pp. 2163–2170, 2014.

[6] P. Polygerinos, Z. Wang, K. C. Galloway, R. J. Wood, and C. J. Walsh, "Soft robotic glove for combined assistance and at-home rehabilitation", *Robotics and Autonomous Systems*, vol. 73, pp. 135–143, 2015.

[7] C. Laschi, M. Cianchetti, B. Mazzolai, L. Margheri, M. Follador, and P. Dario, "Soft robot arm inspired by the octopus", *Advanced Robotics*, vol. 26, no. 7, pp. 709–727, 2012.

[8] A. Villanueva, C. Smith, and S. Priya, "A biomimetic robotic jellyfish (robojelly) actuated by shape memory alloy composite actuators", *Bioinspiration & biomimetics*, vol. 6, no. 3, p. 036 004, 2011.

[9] K. Jung, J. C. Koo, Y. K. Lee, H. R. Choi, *et al.*, "Artificial annelid robot driven by soft actuators", *Bioinspiration & biomimetics*, vol. 2, no. 2, S42, 2007.

[10] M. Wehner, R. L. Truby, D. J. Fitzgerald, B. Mosadegh, G. M. Whitesides, J. Lewis, and R. J. Wood, "An integrated design and fabrication strategy for entirely soft, autonomous robots", 2016.

[11] C. Larson, B. Peele, S. Li, S. Robinson, M. Totaro, L. Beccai, B. Mazzolai, and R. Shepherd, "Highly stretchable electroluminescent skin for optical signaling and tactile sensing", *Science*, vol. 351, no. 6277, pp. 1071–1074, 2016.

[12] N. Lu and K. Dae-Hyeong, "Flexible and stretchable electronics paving the way for soft robotics", *Soft Robotics*, vol. 1, no. 1, pp. 53–62, 2013.

[13] R. Fearing, "Tactile sensing mechanisms", *The International Journal of Robotics Research*, vol. 9, no. 3, pp. 3–23, 1990. eprint: https://doi.org/10.1177/027836499000900301.

[14] M. K. Dobrzynski, R. Pericet-Camara, and D. Floreano, "Contactless deflection sensor for soft robots", *Soft Robotics*, vol. 1, no. 1, pp. 53–62, 2013.

[15] A. Stilli, L. Grattarola, H. Feldmann, H. A. Wurdemann, and K. Althoefer, "Variable stiffness link (vsl): Toward inherently safe robotic manipulators", in *Robotics and Automation (ICRA), 2017 IEEE International Conference on*, IEEE, 2017, pp. 4971–4976.

[16] C. G. Ringwall and A. W. Case Jr, *Tactile sensor*, US Patent 4,306,148, Dec. 1981.

[17] S. Begej, "Planar and finger-shaped optical tactile sensors for robotic applications", *IEEE Journal on Robotics and Automation*, vol. 4, no. 5, pp. 472–484, 1988.

[18] A. Yamaguchi and C. G. Atkeson, "Implementing tactile behaviors using fingervision", in *Humanoid Robotics (Humanoids), 2017 IEEE-RAS 17th International Conference on*, IEEE, 2017, pp. 241–248.

[19] D. Hristu, N. Ferrier, and R. W. Brockett, "The performance of a deformable-membrane tactile sensor: Basic results on geometrically-defined tasks", in *Robotics and Automation, 2000. Proceedings. ICRA'00. IEEE International Conference on*, IEEE, vol. 1, 2000, pp. 508–513.

[20] R. Li, R. Platt, W. Yuan, A. ten Pas, N. Roscup, M. A. Srinivasan, and E. Adelson, "Localization and manipulation of small parts using gelsight tactile sensing", in *Intelligent Robots and Systems (IROS 2014), 2014 IEEE/RSJ International Conference on*, IEEE, 2014, pp. 3988–3993.

[21] C. Chorley, C. Melhuish, T. Pipe, and J. Rossiter, "Development of a tactile sensor based on biologically inspired edge encoding", in *Advanced Robotics, 2009. ICAR 2009. International Conference on*, IEEE, 2009, pp. 1–6.

[22] A. D. Hinitt, J. Rossiter, and A. T. Conn, "Wormtip: An invertebrate inspired active tactile imaging pneumostat", in *Conference on Biomimetic and Biohybrid Systems*, Springer, 2015, pp. 38–49.

[23] H. Yamashita, K. Shibuya, Z. Wang, S. Hirai, J. Nagase, K. Tsutsumi, *et al.*, "Function-selectable tactile sensing system with morphological change", in *System Integration (SII), 2016 IEEE/SICE International Symposium on*, IEEE, 2016, pp. 415–420.

[24] N. J. Ferrier and R. W. Brockett, "Reconstructing the shape of a deformable membrane from image data", *The International Journal of Robotics Research*, vol. 19, no. 9, pp. 795–816, 2000.

[25] W. Yuan, R. Li, M. A. Srinivasan, and E. H. Adelson, "Measurement of shear and slip with a gelsight tactile sensor", in *Robotics and Automation (ICRA), 2015 IEEE International Conference on*, IEEE, 2015, pp. 304–311.

[26] L. Cramphorn, B. Ward-Cherrier, and N. F. Lepora, "Tactile manipulation with biomimetic active touch", in *Robotics and Automation (ICRA), 2016 IEEE International Conference on*, IEEE, 2016, pp. 123–129.

[27] G. Moy, C. Wagner, and R. S. Fearing, "A compliant tactile display for teletaction", in *Robotics and Automation, 2000. Proceedings. ICRA'00. IEEE International Conference on*, IEEE, vol. 4, 2000, pp. 3409–3415.

[28] D. Vella, A. Ajdari, A. Vaziri, and A. Boudaoud, "The indentation of pressurized elastic shells: From polymeric capsules to yeast cells", *Journal of the Royal Society Interface*, rsif20110352, 2011.

[29] K. L. Johnson, *Contact mechanics*. Cambridge university press, 1987.

[30] R. D. Howe and M. R. Cutkosky, "Sensing skin acceleration for slip and texture perception", in *Robotics and Automation, 1989. Proceedings., 1989 IEEE International Conference on*, IEEE, 1989, pp. 145–150.

[31] C. Melchiorri, "Slip detection and control using tactile and force sensors", *IEEE/ASME transactions on mechatronics*, vol. 5, no. 3, pp. 235–243, 2000.

[32] E. Holweg, H. Hoeve, W. Jongkind, L. Marconi, C. Melchiorri, and C. Bonivento, "Slip detection by tactile sensors: Algorithms and experimental results", in *Robotics and Automation, 1996. Proceedings., 1996 IEEE International Conference on*, IEEE, vol. 4, 1996, pp. 3234–3239.

[33] J. S. Son, E. A. Monteverde, and R. D. Howe, "A tactile sensor for localizing transient events in manipulation", in *Robotics and Automation, 1994. Proceedings., 1994 IEEE International Conference on*, IEEE, 1994, pp. 471–476.

[34] J. M. Romano, K. Hsiao, G. Niemeyer, S. Chitta, and K. J. Kuchenbecker, "Human-inspired robotic grasp control with tactile sensing", *IEEE Transactions on Robotics*, vol. 27, no. 6, pp. 1067–1079, 2011.

[35] Z. Su, K. Hausman, Y. Chebotar, A. Molchanov, G. E. Loeb, G. S. Sukhatme, and S. Schaal, "Force estimation and slip detection/classification for grip control using a biomimetic tactile sensor", in *Humanoid Robots (Humanoids), 2015 IEEE-RAS 15th International Conference on*, IEEE, 2015, pp. 297–303.

[36] M. Kaboli, K. Yao, and G. Cheng, "Tactile-based manipulation of deformable objects with dynamic center of mass", in *Humanoid Robots (Humanoids), 2016 IEEE-RAS 16th International Conference on*, IEEE, 2016, pp. 752–757.

[37] K. Y. Goldberg and R. Bajcsy, "Active touch and robot perception", *Cognition and Brain Theory*, vol. 7, no. 2, pp. 199–214, 1984.

[38] P. R. Sinha and R. Bajcsy, "Active exploration of surfaces for legged locomotion of robots", 1990.